*Journal of The Electrochemical Society*, **151** (4) F87-F91 (2004)
0013-4651/2004/151(4)/F87/5/$7.00 © The Electrochemical Society, Inc.

# Studies on Ferroelectric Properties of Sol-Gel Derived $Pb(Zr_{0.53}Ti_{0.47})O_3$ Using $Ba_{0.5}Sr_{0.5}RuO_3$ as the Conductive Electrodes

**Y. K. Wang,[a] C. H. Huang,[a] T. Y. Tseng,[a,z] and Pang Lin[b]**

[a]*Department of Electronics Engineering and Institute of Electronics, and* [b]*Institute of Materials Science and Engineering, National Chiao Tung University, Hsinchu 30050, Taiwan*

$Pb(Zr_{0.53}Ti_{0.47})O_3$ (PZT) thin films with a (110) preferred orientation were prepared on $Ba_{0.5}Sr_{0.5}RuO_3$ (BSR)/Ru/$SiO_2$/Si substrates using a sol-gel method. The oxide bottom electrode, BSR, was fabricated at various temperatures on Ru/$SiO_2$/Si substrates by rf sputtering. The annealed PZT films on BSR/Ru/$SiO_2$/Si substrates exhibited improved crystallinity. The electrical properties of PZT films, such as the electric field (*E*) induced variations of the leakage current density, the dielectric constant, and the polarization were strongly dependent on the processing temperatures of the PZT films as well as the bottom oxide electrode. A typical PZT thin film annealed at 650°C on the BSR electrode, which was deposited at 450°C on the Ru/$SiO_2$/Si substrate by a sputtering technique, has a leakage current of $2.7 \times 10^{-7}$ A/cm$^2$ at an applied electric field of 500 kV/cm and a dielectric constant of 968. From the polarization-electric field characteristics, the remanent polarization and coercive field of the PZT were found to be 38.9 μC/cm$^2$ and 59.6 kV/cm, respectively, at an applied voltage of 5 V. The PZT films exhibited fatigue-free characteristics up to $\sim 1.0 \times 10^{12}$ switching cycles under 5 V bipolar pulses.
© 2004 The Electrochemical Society. [DOI: 10.1149/1.1667522] All rights reserved.

Manuscript submitted January 23, 2003; revised manuscript received October 29, 2003. Available electronically March 3, 2004.

Pb(Zr,Ti)$O_3$ (PZT) thin films have attracted attention because of the excellent ferroelectric properties, which can be exploited for applications in nonvolatile random access memories (NVRAMs) and dynamic random access memories (DRAMs).[1-4] However, many reports have indicated that the PZT thin films have serious fatigue problems when deposited on metal electrodes because of the degradation of the film/electrode interface, which results in a relatively shorter number of switching cycles.[5-7] The conductive metallic oxide electrodes, such as $RuO_2$,[8] $IrO_2$,[9] $(La_{0.5},Sr_{0.5})CoO_3$,[10] $BaRuO_3$ (BRO),[11] $SrRuO_3$ (SRO),[12] and $Ba_xSr_{1-x}RuO_3$ (BSR),[13] have been found to improve the fatigue properties of the PZT capacitors. The polarization fatigue, which arises out of repeated switching cycles, gets suppressed at a ferroelectric film/oxide electrode heterostructure as the oxide electrodes act as sinks for the oxygen vacancies. The selection of electrode materials will also affect the microstructure and the electrical properties of the thin films. Moreover, the perovskite oxide electrodes should have similar lattice parameter and crystal structure with PZT thin films as these characteristics decide the formation of the chemically and thermally stable PZT/perovskite oxide electrode interface, which eventually enhance the ferroelectric characteristics of PZT films.[14] However, it is very difficult to deposit preferentially oriented PZT or BSR films on silicon substrates. In most of the studies on epitaxial PZT or BSR thin films, the films were deposited on $SrTiO_3$ (STO) or $LaAlO_3$ (LAO) substrates.[15-17] In our earlier study,[18] the (110)-oriented SRO oxide electrodes were deposited on an Ru/$SiO_2$/Si substrate at a low temperature, subsequently (110)-oriented PZTs were grown on SRO(110)/Ru/$SiO_2$/Si substrates. The PZT films on SRO(110)/Ru/$SiO_2$/Si exhibited improved ferroelectric properties. Obviously, the enhancement in the ferroelectric properties of PZT deposited on the perovskite oxide electrodes can be obtained and would be of interest for future ferroelectric memory applications. However, in our previous study, a detailed investigation of structure and ferroelectric properties was not carried out. In this study, we prepared highly oriented (110) PZT thin films on conducting oxides, namely (Bs,Sr)$RuO_3$ (BSR), as bottom electrodes. Thin films of BSR with (110) preferred orientation were sputter-deposited on Ru/$SiO_2$/Si substrates. The structure and the ferroelectric properties of PZT films were studied in detail.

[z] E-mail: tseng@cc.nctu.edu.tw

## Experimental

The initial attempt to prepare the BSR target through a solid-state reaction using stoichiometric amounts of a $RuO_2$, $SrCO_3$, and $BaCO_3$ mixture as the starting materials was not successful. Subsequently, $BaRuO_3$ and $SrRuO_3$ were prepared separately through a solid-state reaction using $BaCO_3$, $SrCO_3$, and $RuO_2$ as starting materials and then mixed and different ratios of the end members used to form the BSR solid solution were calcined. The experimental conditions employed for the synthesis of BRO and SRO phases can be summarized as follows: stoichiometric amounts of $RuO_2$ and $BaCO_3$ were mixed in a ball mill and calcined at 1000°C for 4 h to from single-phase $BaRuO_3$ (BRO) powder. Similarly, the single-phase $SrRuO_3$ was prepared from high purity $RuO_2$ and $SrCO_3$ powders by calcining the well-mixed reactant mixture for 4 h at 1250°C. The phase formations of both end members were confirmed by X-ray diffraction (XRD). In order to prepare the solid-solution target, BSR, with the desired composition, $Ba_{0.5}Sr_{0.5}RuO_3$, the stoichiometric amounts of BRO and SRO were mixed in a ball mill followed by calcination at 1500°C. However, the XRD characterization of the 1500°C calcined powder did not confirm the formation of the BSR phase. Finally, the BSR target was fabricated by mixing different ratios of well-crystallized BRO and SRO phases. In our experiments, we used the low-temperature calcined (600°C, 4 h) mixture of BRO and SRO powders as the target material. Based on XRD results (not shown here), such a 600°C calcined powder target is the mixture of BRO and SRO phases.

The BSR thin films were deposited on Ru/$SiO_2$/Si(100) substrates at various temperatures by rf magnetron sputtering. The thermally oxidized silicon dioxide layer ($SiO_2$, 100 nm thick) was employed to suppress the reaction between Ru and silicon. The 50 nm thick Ru metal films were deposited at 400°C using rf sputtering. The deposition conditions and the resultant thicknesses of Ru and BSR films are listed in Table I. The PZT films with a thickness of 200 nm were grown by a sol-gel method. The annealing of the films was performed in a tube furnace at various temperatures ranging from 500 to 700°C under $O_2$ atmosphere. The BSR top electrodes with an area of $4.9 \times 10^{-5}$ cm$^2$ were sputter deposited onto the PZT films at room temperature, and then thermally treated at 400°C for 10 min to reduce the interface defects during sputtering. The crystallinity of the films was examined by XRD (Siemens D5000), with Cu Kα radiation. The surface morphology and the microstructure were observed by using atomic force microscope (AFM, Digital Instruments Nanoscope III) and scanning electron microscope

Downloaded on 2014-04-27 to IP 140.113.38.11 address. Redistribution subject to ECS terms of use (see ecsdl.org/site/terms_use) unless CC License in place (see abstract).

**Table I. The deposition conditions and thicknesses of Ru and BSR films.**

| Films | Ru | BSR |
|---|---|---|
| Target | Metallic Ru | SRO and BRO packed powder |
| Substrate temperature | 400°C | 300-500°C, room temperature |
| Sputtering gas | Ar | $Ar/O_2 = 3/1$ |
| RF power (W) | 100 | 100 |
| Working pressure (mTorr) | 10 | 10 |
| Film thickness (nm) | 50 | 300 |

(SEM, Hitachi S-4700), respectively. The capacitance-voltage (C-V) characteristics were measured with an impedance-gain-phase analyzer (Hewlett-Packard, HP, 4194A) at 100 kHz. The current-voltage ($I$-$V$) measurements were performed by using a semiconductor parameter analyzer (HP4156B). The ferroelectric properties of the films were measured using a RT66A ferroelectric tester (Radiant Technologies, Inc.).

## Results and Discussion

Figure 1 shows the XRD patterns of BSR films deposited on $Ru/SiO_2/Si$ substrates at various temperatures. The deposited BSR films have a preferred (110) orientation with the well-defined peaks appearing at deposition temperatures as low as 300°C, and the peak intensity of (110)-oriented BSR films increases with increasing deposition temperature. Similar results were observed when the SRO was deposited on $Ru/SiO_2/Si$ substrates.[18] We also observed the (110) peak of the $RuO_2$ phase for the films deposited at 450°C due to the oxidation reaction at the interface between BSR and Ru at high deposition temperature. The additional peak corresponding to Ru(100) appears at deposition temperatures in the range from 450 to 500°C.

The XRD patterns of the PZT films deposited on BSR (450°C deposited)/$Ru/SiO_2/Si$ substrates and annealed at temperatures ranging from 400 to 700°C are shown in Fig. 2. A strong (110) preferred orientation appeared in PZT films annealed at 450°C, and this preferred orientation is further enhanced by increasing the annealing temperature up to 700°C. We observed from our XRD results, that the PZT-(110) films crystallized on the 300°C deposited BSR electrodes. The (110)-oriented BSR bottom electrode could enhance the crystallization of PZT films to form the preferred orientation of (110). In addition, all of the XRD patterns of PZT films annealed at high temperature could find the (110) orientation of $RuO_2$ even though the bottom electrode was deposited at lower than 450°C. The XRD patterns of the BSR films, which were deposited on $Ru/SiO_2/Si$ substrates at various temperatures and then furnace annealed at 600°C in $O_2$, that is, the same heat-treatment with PZT

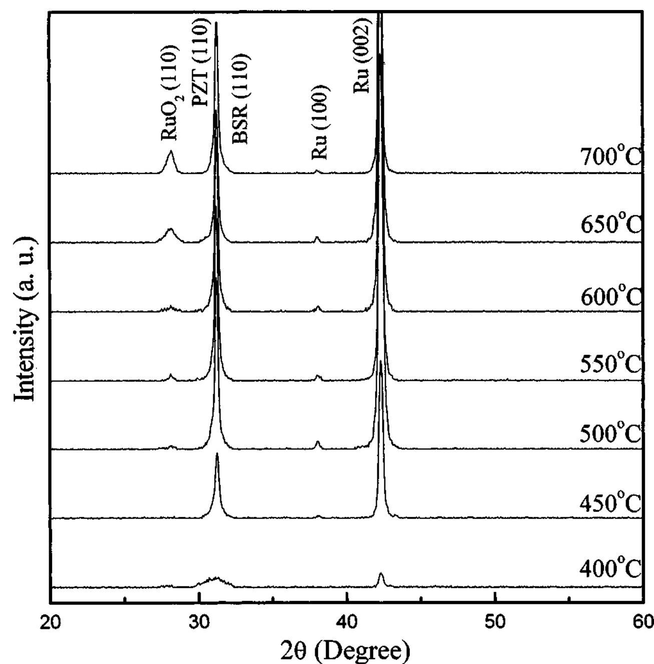


**Figure 2.** XRD patterns of PZT films deposited on 450°C-grown BSR/$Ru/SiO_2/Si$ substrates and annealed at the various temperatures indicated.

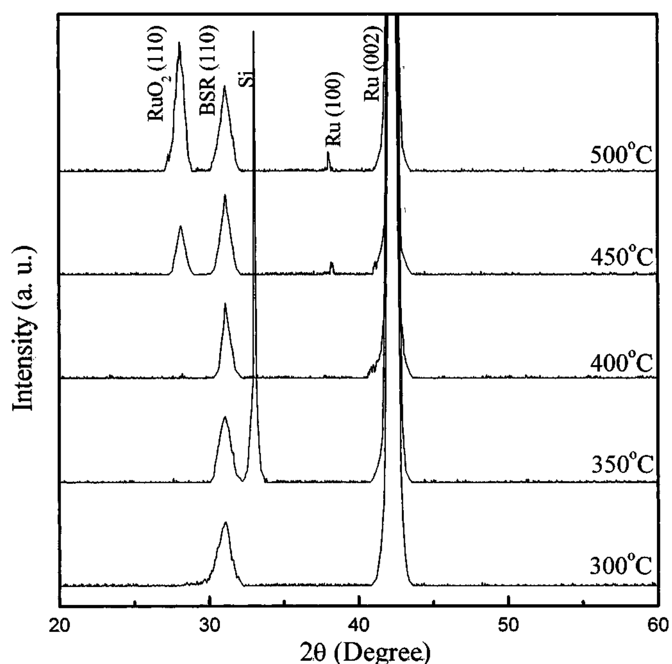


**Figure 1.** XRD patterns of BSR films deposited on $Ru/SiO_2/Si$ substrates at the various temperatures indicated.

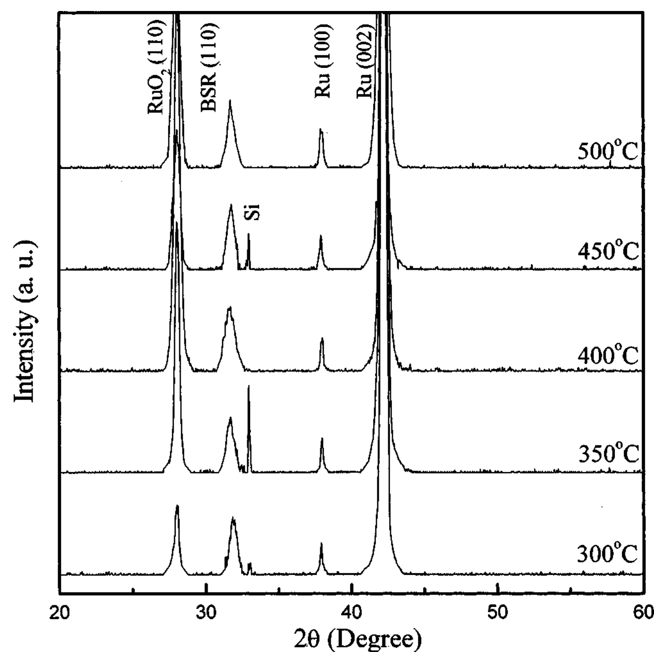


**Figure 3.** XRD patterns of BSR films deposited on $Ru/SiO_2/Si$ substrates at the various temperatures indicated and then furnace-annealed at 600°C under $O_2$ atmosphere.

Downloaded on 2014-04-27 to IP 140.113.38.11 address. Redistribution subject to ECS terms of use (see ecsdl.org/site/terms_use) unless CC License in place (see abstract).

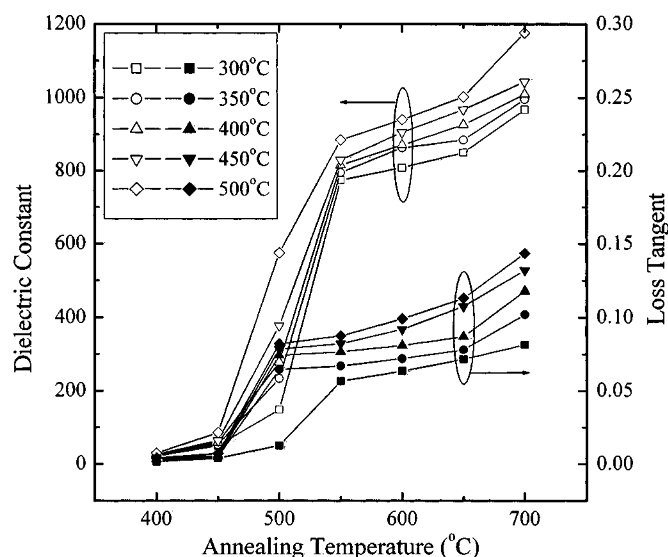


**Figure 4.** Dielectric constant and loss tangent of PZT thin films annealed at various temperatures on the BSR bottom electrodes deposited at various temperatures.

films, are indicated in Fig. 3. It appears the $RuO_2(110)$ and the Ru(100) peaks in addition to the BSR(110) and the Ru(002) peaks. The formation of $RuO_2$ is attributed to the interface reaction between Ru and BSR leading to oxidation of the Ru at high annealing temperatures. The $RuO_2(110)$ and the Ru(100) formation would not affect the crystallization of the PZT films, because the BSR crystallization directly influenced the PZT thin-film growth.

The dielectric constant and the loss tangent of the PZT films as a function of the annealing temperature and BSR electrode deposition temperature are depicted in Fig. 4. The dielectric constant and the loss tangent increase with the increase in annealing temperature of the PZT films and deposition temperature of the BSR bottom electrodes. When the annealing temperature is lower than 450°C, the dielectric constants of the PZT films are small because they are amorphous. When the annealing temperature is higher than 450°C, the PZT films are well crystallized and have high dielectric constants. The high dielectric constant for the high-temperature annealed PZT films is attributed to better crystallinity, larger grain size, and higher polarization of the highly oriented films. The evidence of high annealing temperature enhancement of the grain growth of the PZT films is shown in Fig. 5. On the other hand, the better crystallization of the BSR bottom electrodes could enhance the crystallization of the PZT films and consequently increase their dielectric constants. Figure 6 shows the leakage current density of the PZT films deposited on BSR (450°C deposited)/Ru/$SiO_2$/Si substrates. The symmetry of the curves indicates the same structure and material for both the top and the bottom electrodes. The leakage current density of the PZT film annealed at 400°C has a low value of $5 \times 10^{-10}$ A/cm$^2$ at 750 kV/cm because of its amorphous nature, whereas the 700°C-annealed PZT has a high leakage current of $1.3 \times 10^{-6}$ A/cm$^2$ at the same electric field. The leakage current increases with elevated annealing temperature, because the column grains are easily grown in the PZT films at high temperatures (Fig. 7), which supply short-circuit paths under the applied bias. The interface reac-

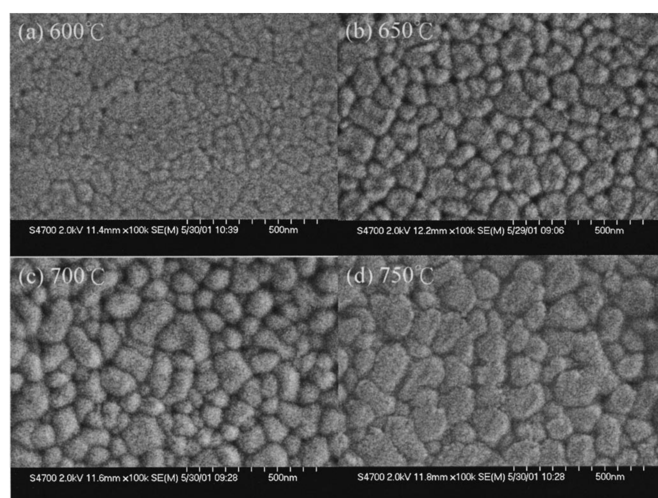


**Figure 5.** SEM images of PZT films deposited on the 450°C-grown BSR/Ru/$SiO_2$/Si substrates annealed at (a) 600, (b) 650, (c) 700, and (d) 750°C.

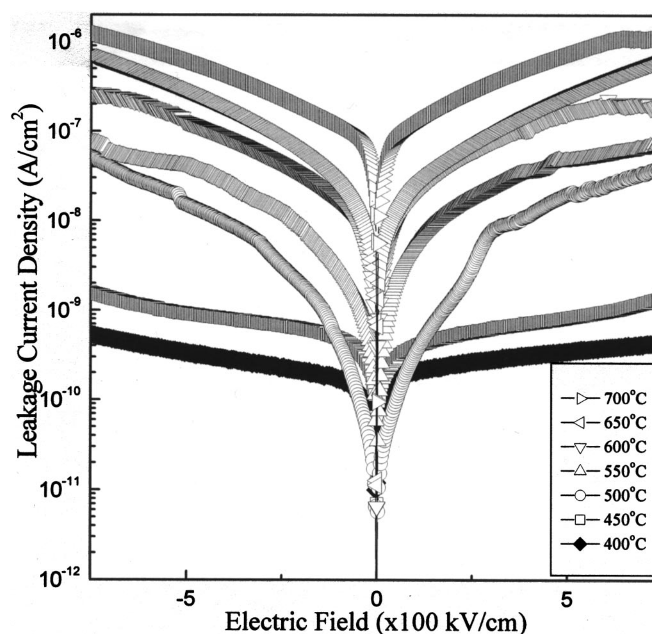


**Figure 6.** The *I-V* characteristics of PZT thin films deposited on the 450°C-grown BSR/Ru/$SiO_2$/Si substrates and annealed at the various temperatures indicated.

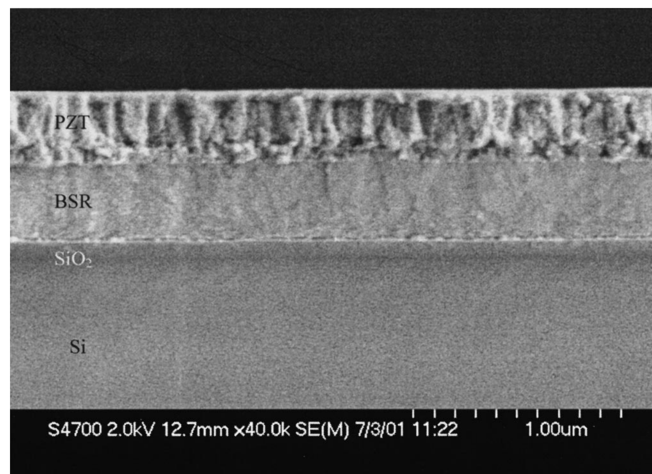


**Figure 7.** SEM cross section of the PZT film deposited on the 450°C grown BSR/Ru/$SiO_2$/Si substrate and annealed at 700°C.

Downloaded on 2014-04-27 to IP 140.113.38.11 address. Redistribution subject to ECS terms of use (see ecsdl.org/site/terms_use) unless CC License in place (see abstract).

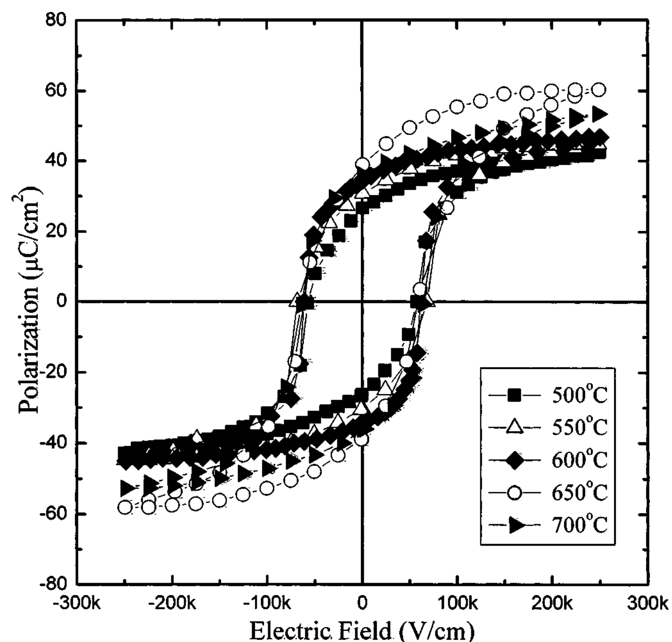


**Figure 8.** Polarization *vs.* electric field characteristics of PZT thin films deposited on a 450°C BSR bottom electrode and annealed at various temperatures.

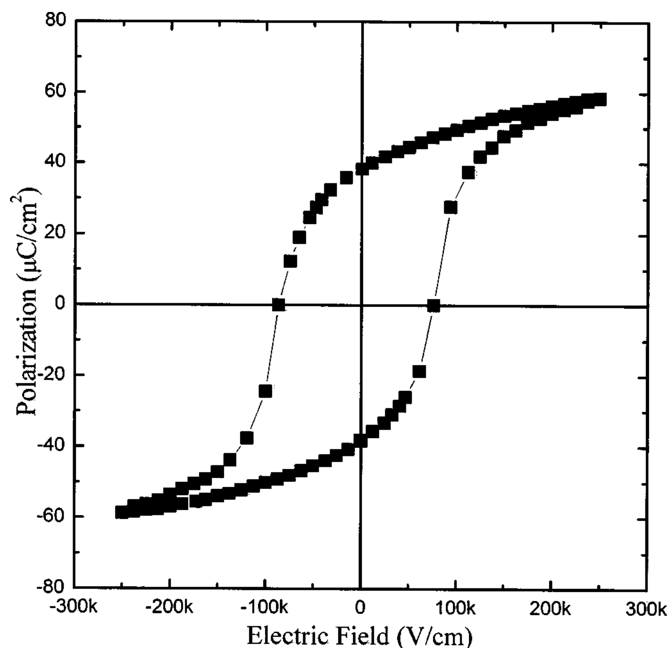


**Figure 10.** Polarization *vs.* electric field characteristic of the PZT thin film deposited on $CeO_2$ (15 nm)/BSR/$SiO_2$/Si substrate and annealed at 700°C.

tions between BSR and PZT films might also deteriorate the PZT performance. In addition, lead loss easily occurs in the high annealing temperatures, which might induce the increase of the leakage current and the loss tangent. The deposition temperature of the BSR electrodes also affects the leakage current of the PZT thin films. The better crystallized BSR electrode would lead to the PZT films having a larger column grain size, which is the main cause for the larger leakage current.

The polarization-electric field hysteresis loops for the PZT films on the 450°C-deposited BSR electrodes, which were annealed at various temperatures, are illustrated in Fig. 8. The remanent polarization ($P_r$) of PZT films increases with an increase in annealing temperature up to 650°C, as a result of better crystallization of the PZT films. The 650°C-annealed PZT films have a relatively high value of $P_r$, 38.9 μC/cm$^2$. The $P_r$ of the 700°C annealed PZT films were lower than that of the 650°C-annealed-PZT, which may be due to the interfacial reaction between oxide and electrode. To verify this point, the secondary ion mass spectroscopy (SIMS) analysis of the interface of the PZT/BSR heterostructure was carried out, and its result is indicated in Fig. 9. The interdiffusion between PZT film and the BSR electrode indeed occurred at the high temperature of 700°C, which results in a reduction of $P_r$ values. We also attempted to deposit a thin $CeO_2$ (15 nm) between the 700°C-annealed-PZT film and the bottom electrode and then measure its hysteresis loop. The result in Fig. 10 indicates that the $P_r$, 38.2 μC/cm$^2$ of 700°C-annealed PZT films using the $CeO_2$ buffer layer is larger than 36.1 μC/cm$^2$ without the $CeO_2$ layer. Obviously, the $CeO_2$ provides a diffusion barrier to reduce ferroelectric and oxide bottom electrode interdiffusion. Some studies reported that the strontium atoms diffused into ferroelectric films easily, which degrades the ferroelectric properties.[19] It is supposed that strontium and barium ions diffused into PZT (Fig. 9) have been obstructed the by $CeO_2$ buffer layer, resulting in higher $P_r$ of the PZT film. The $P_r$ values of the annealed PZT films on various temperature-deposited BSR electrodes are summarized in Table II. The fatigue characteristics of the 650°C-annealed-PZT films are depicted in Fig. 11, which indicates that the

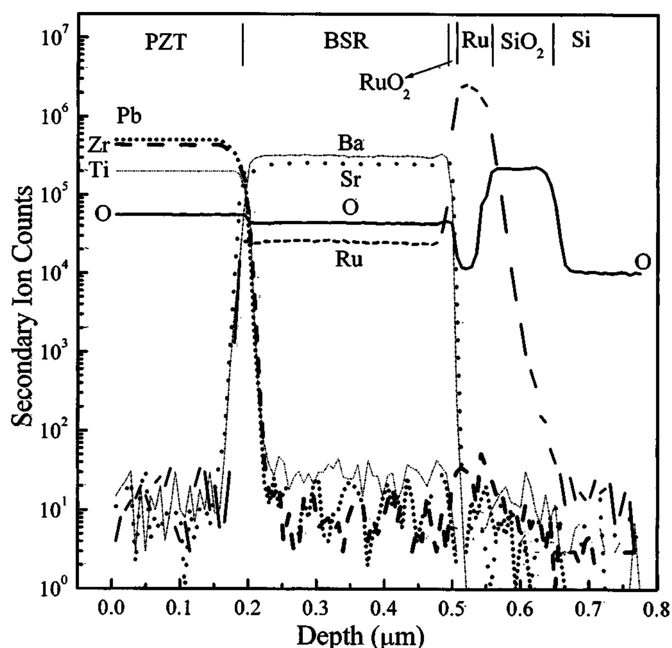


**Figure 9.** The SIMS analysis of the PZT thin film on the 450°C-deposited BSR bottom electrode and then annealed at 700°C.

**Table II. The remanent polarization values of various temperature-annealed PZT films deposited on various temperature prepared BSR electrodes.**

| Remanent polarization (μ C/cm$^2$) | | $Ba_{0.5}Sr_{0.5}RuO_3$ deposition temperature (°C) | | | | |
|---|---|---|---|---|---|---|
| | | 300 | 350 | 400 | 450 | 500 |
| PZT annealing temperature (°C) | 500 | 10.8 | 15.8 | 19.2 | 24.4 | 28.8 |
| | 550 | 15.5 | 23.3 | 26.0 | 30.5 | 33.5 |
| | 600 | 18.1 | 29.3 | 32.8 | 33.8 | 38.5 |
| | 650 | 21.7 | 32.5 | 35.6 | 38.9 | 43.5 |
| | 700 | 23.9 | 28.8 | 32.6 | 36.1 | 41.2 |

Downloaded on 2014-04-27 to IP 140.113.38.11 address. Redistribution subject to ECS terms of use (see ecsdl.org/site/terms_use) unless CC License in place (see abstract).

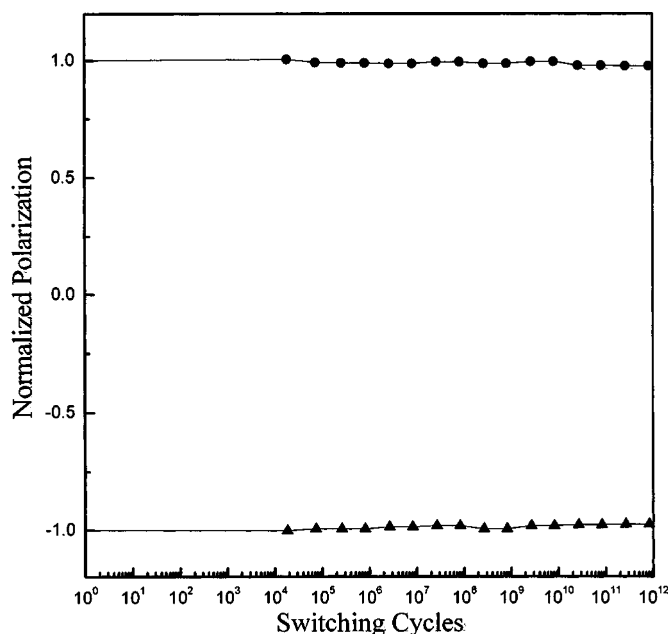


**Figure 11.** Fatigue behavior of the 650°C-annealed PZT thin film which was deposited at 450°C on BSR/Ru/$SiO_2$/Si with a 100 kHz bipolar square wave peak-to-peak fatigue voltage of 10 V.

highly (110) oriented PZT films deposited on BSR/Ru/$SiO_2$/Si substrates do not show any deterioration after $\sim 10^{12}$ switching cycles.

## Conclusions

We have demonstrated the deposition and the characterization of the PZT thin films with a (110)-preferred orientation on BSR bottom electrodes by a sol-gel method. The bottom electrode, BSR, was deposited by rf sputtering on Ru/$SiO_2$/Si substrates. A low leakage current has been recorded for the PZT films annealed at lower temperatures. However, the leakage current increased for the films annealed at higher temperatures. The value of the dielectric constant and the $P_r$ were also increased with raising the annealing temperature up to 650°C. However, the $P_r$ value decreased on further increasing the annealing temperature, which was attributed to strontium and barium ions diffused into PZT films. The PZT films were fatigue-free even after $\sim 10^{12}$ switching cycles.

## Acknowledgment

This work was supported by the National Science Council R. O. C. under contract no. NSC 91-2219-E-009-028.

*National Chiao Tung University assisted in meeting the publication costs of this article.*

## References


1. J. T. Evans, Jr. and R. Womack, *IEEE J. Solid-State Circuits,* **23**, 1171 (1998).
2. W. A. Geideman, *IEEE Trans. Ultrason. Ferroelectr. Freq. Control,* **38**, 704 (1991).
3. J. F. Scott and C. A. Paz de Araujo, *Science,* **246**, 1400 (1989).
4. T. Y. Tseng, in *Proceedings of International Electron Devices and Materials Symposia*, Hsinchu, Taiwan, 2-5, 89 (1996).
5. K. R. Bellur, H. N. Al-Shareef, S. H. Rou, K. D. Gifford, O. Auciello, and A. I. Kingon, in *Proceedings of the 8th IEEE International Symposium on the Applications of Ferroelectrics*, 448 (1992).
6. H. M. Duiker, P. D. Beale, J. F. Scott, C. A. Paz de Araujo, B. M. Melnick, J. D. Cuchiaro, and L. D. McMillan, *J. Appl. Phys.,* **68**, 5783 (1990).
7. P. K. Larsen, G. J. M. Dormans, D. J. Taylor, and P. J. van Veldhoven, *J. Appl. Phys.,* **76**, 2405 (1994).
8. G. J. Norga, D. J. Wouters, A. Bartic, Laura Fè, and H. E. Maes, in *Proceedings of the 11th IEEE International Symposium on Applications of Ferroelectrics*, 3-6 (1998).
9. T. Nakamura, Y. Nakao, A. Kamisawa, and H. Takasu, *Jpn. J. Appl. Phys., Part 1,* **33**, 5207 (1994).
10. R. Ramesh, T. Sands, and V. G. Keramidas, *J. Electron. Mater.,* **23**, 19 (1994).
11. S.-M. Koo, L.-R. Zheng, and K. V. Rao, *J. Electron. Mater.,* **14**, 3833 (1999).
12. C. Guerrero, J. Roldán, C. Ferrater, M. V. Garcia-Cuenca, F. Sánchez, and M. Varela, *Solid-State Electron.,* **45**, 1433 (2001).
13. D.-K. Choi, B.-S. Kim, S.-Y. Son, S.-H. Oh, and K.-W. Park, *J. Appl. Phys.,* **86**, 3347 (1999).
14. K. P. Jayadevan and T. Y. Tseng, *J. Mater. Sci.: Mater. Electron.,* **13**, 439 (2002).
15. J. H. Kim, A. T. Chien, F. F. Lange, and L. Wills, *J. Mater. Res.,* **14**, 1190 (1999).
16. C. M. Foster, G. R. Bai, R. Csencsits, J. Vetrone, R. Jammy, L. A. Wills, E. Carr, and J. Amano, *J. Appl. Phys.,* **81**, 2349 (1997).
17. K. Nagashima, M. Aratani, and H. Funahubo, *J. Appl. Phys.,* **89**, 4517 (2001).
18. Y. K. Wang, T. Y. Tseng, and P. Lin, *Appl. Phys. Lett.,* **80**, 3790 (2002).
19. S.-M. Yoon, E. Tokumitsu, and H. Ishiwara, *Appl. Surf. Sci.,* **117/118**, 447 (1997).


Downloaded on 2014-04-27 to IP 140.113.38.11 address. Redistribution subject to ECS terms of use (see ecsdl.org/site/terms_use) unless CC License in place (see abstract).